Hollow Structures

DOI: 10.1002/anie.201202877

Unusual Formation of Single-Crystal Manganese Sulfide Microboxes Co-mediated by the Cubic Crystal Structure and Shape

*Lei Zhang, Liang Zhou, Hao Bin Wu, Rong Xu, and Xiong Wen (David) Lou**

Hollow micro and nanostructures with well-defined interior voids, low density, and surface permeability have attracted considerable interest because of their widespread applications in nanoreactors, drug delivery, gas sensors, and energy storage and conversion.[1–6] More recently, efforts have been dedicated to the rational design of nonspherical hollow structures with well-defined morphologies in view of their unique physical and chemical properties.[7–10] Although templating strategies are versatile for the synthesis of many hollow spherical structures, controllable preparation of nonspherical hollow structures still suffers from many difficulties ranging from forming uniform coating around high curvature surfaces to the paucity of nonspherical templates available.[1] Recently, many novel approaches based on different principles, such as galvanic replacement,[11,12] chemical etching,[13–15] the Kirkendall effect,[16,17] solid-state decomposition,[18] and self-assembly,[9,19] have been employed for synthesizing nonspherical hollow structures of various materials, such as noble metals, transition metal oxides, and sulfides. In most cases, nonspherical hollow cavities are created though solution-phase methods by selective dissolution of the interior materials.[11–13,18] Although the solution methods have enabled the preparation of hollow structures with nonspherical cavities, the resulting hollow structures are mostly characterized by such features as rough surfaces, polycrystallinity, non-uniformity in shell thickness, poorly defined composition, and broken shells.[12,20]

Herein, we demonstrate a facile H_2S gas sulfidation route for preparing uniform microboxes of metal sulfides with single-crystalline shells. We choose MnS as an example to demonstrate the concept in view of the limited success in synthesizing nonspherical MnS hollow structures and its wide technological applications in various fields. The MnS microboxes exhibit improved electrochemical performance when evaluated as an anode material for lithium ion batteries (LIBs).

Figure 1a illustrates the shape-dependent topotactic growth process for the formation of single-crystalline MnS microboxes. Uniform $MnCO_3$ microcubes (Supporting Information, Figure S1) prepared by a co-precipitation method are employed as the precursor.[21] A sulfidation treatment at 800 °C under H_2S atmosphere is utilized to convert the $MnCO_3$ microcubes into single-crystalline MnS microboxes. The whole formation process can be generally divided into three stages. In stage I, the $MnCO_3$ microcubes begin to transform into porous MnS microcubes with the face-centered cubic (FCC) crystal structure at a relatively low temperature of about 350 °C by the reaction: $MnCO_3 + H_2S \rightarrow MnS + H_2O + CO_2$. As the temperature increases, the MnS nanocrystals at the surface region of the porous microcubes grow into a dense single-crystalline shell, which well inherits the overall cubic morphology owing to the intrinsic FCC crystal structure and the topotactic effect. At the same time, the MnS nanocrystals in the core region continuously diffuse out and re-crystallize on the single-crystalline shell at high temperature (stage II). Through this mechanism, the inner core materials evacuate outward continuously, finally generating a single cavity in the center (stage III). Compared with the widely used solution methods, in which the concentration of the precursors is usually very low, the present solid-state method provides a more feasible route for large-scale synthesis of uniform hollow structures.

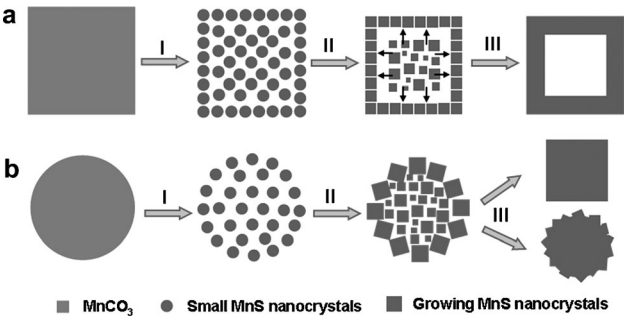

Figure 1. The formation of single-crystal MnS microboxes (a) and irregular cubelike microparticles (b). See text for details.

The crystallographic structure and phase purity of the MnS microboxes were examined by X-ray powder diffraction (XRD). As can be seen from Figure 2a, all of the diffraction peaks can be assigned to FCC MnS (JCPDS Card No. 72-1534; space group: $Fm3m$, $a = b = c = 5.240$ Å). No diffraction peaks from residues or impurities have been detected, indicating the high purity of the product. Field-emission scanning electron microscopy (FESEM) and transmission electron microscopy (TEM) studies reveal the morphology and detailed structure of the products. A panoramic FESEM image (Figure 2b) shows that the sample consists of uniform microcubes with size of about 2.5 μm without aggregation. The FESEM image of a cracked microbox is shown in Figure 2c, clearly showing the hollow interior. The detailed

[*] Dr. L. Zhang, Dr. L. Zhou, H. B. Wu, Prof. R. Xu, Prof. X. W. (David) Lou
School of Chemical and Biomedical Engineering
Nanyang Technological University
70 Nanyang Drive, Singapore 637457 (Singapore)
E-mail: xwlou@ntu.edu.sg
Homepage: http://www.ntu.edu.sg/home/xwlou/

Supporting information for this article is available on the WWW under http://dx.doi.org/10.1002/anie.201202877.

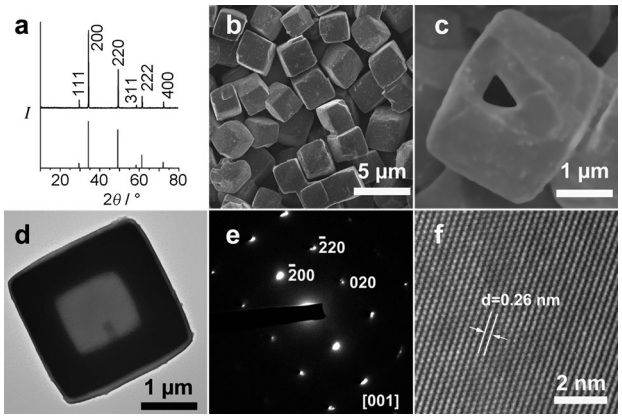

Figure 2. Characterization of single-crystal MnS microboxes prepared at 800 °C. a) XRD pattern (lower: JCPDS card no. 72-1534); b,c) FESEM images; d) TEM image; e) SAED pattern; f) HRTEM image.

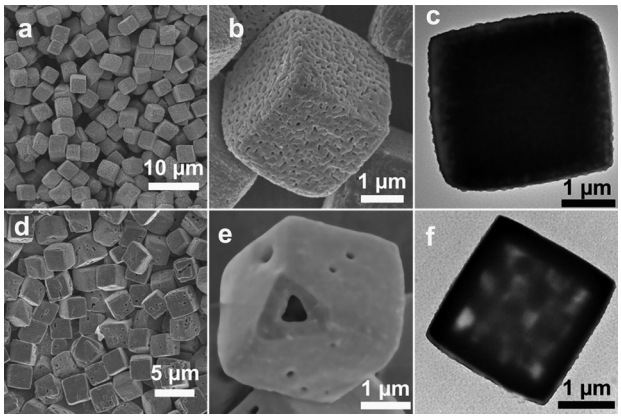

Figure 3. a), b), d), e) FESEM and c), f) TEM images of porous MnS microcubes obtained at 350 °C (a–c) and hollow MnS microcubes obtained at 600 °C (d–f).

structure of the products is further elucidated by TEM, high-resolution TEM (HRTEM), and selected-area electron diffraction (SAED). In agreement with the above FESEM findings, a well-defined cubic void can be observed inside each microcube in the low-magnification TEM image (Figure 2 d). The inner cavity is clearly revealed by the sharp contrast between the center and the edge. The size of the hollow cavity and the thickness of the shell are determined to be about 1.2 μm and 0.6 μm, respectively. The SAED pattern (Figure 2 e) obtained from different square faces of intentionally broken microboxes always shows the same set of diffraction spots. This observation evidently suggests the single-crystalline characteristic of the MnS microboxes, although we are not able to get a SAED pattern based on a whole microbox because of its relatively large size. The SAED pattern can be indexed to the [001] zone axis of cubic MnS. A combination of the FESEM/TEM and SAED results suggests that the MnS microboxes are bounded by six {100} facets. Figure 2 f shows a HRTEM image of the MnS shell, where the {200} lattice fringes (2.6 Å) can be clearly observed. We further explored the generality of this novel formation of metal sulfide microboxes at high temperature. Encouragingly, microboxes of Co- and Ni-doped MnS can also be successfully fabricated by using Co- and Ni-doped $MnCO_3$ microcubes as the precursor, respectively (see Supporting Information, Figure S2).

To understand the formation mechanism, the samples were treated at different temperatures to investigate the structural evolution of the microcubes. At a relatively low temperature of 350 °C, porous MnS microcubes are generated with very uniform porous structures (Figure 3 a, b; Supporting Information, Figure S3). The TEM examination (Figure 3 c) confirms that these porous microcubes do not have large cavities in the center. At a higher temperature of 600 °C, MnS microcubes with a single-crystalline outer shell and many small interior chambers are formed (Figure 3 d–f). Another observation is that the surface of the MnS microcubes prepared at 350 °C is very rough, while that of the sample prepared at 600 °C is quite smooth, although there are still some small holes on the surface. These holes may be considered as defects of the single-crystalline shell. Note that the small MnS nanocrystals in the core region are packed more loosely than the single-crystalline outer shell. As a result, they will possess much higher surface energy, which in turn leads to a strong tendency to migrate and relocate to the outer shell.[22,23] It is also worth noting that the hollowing process is accompanied by crystal growth of MnS particles, and it is relatively easy for the primary particles on the outer surface to grow into a single-crystalline shell mediated by its intrinsic cubic crystal structure and the topotactic effect. With the continuous evacuation of inner particles and the crystallography-driven topotactic growth of a single-crystalline outer shell, microboxes with single-crystalline shells can be finally produced at high temperature. Indeed, this interesting evolution is accompanied by a drastic reduction in the Brunauer–Emmett–Teller (BET) specific surface area from $10.2\ m^2 g^{-1}$ for porous microcubes to only $1.6\ m^2 g^{-1}$ for microboxes (Supporting Information, Figure S4).

To verify the proposed formation of MnS microboxes co-mediated by crystal structure and shape, we also synthesized $MnCO_3$ micospheres with the same crystal structure and similar size as a counterexample (Supporting Information, Figure S5). Porous MnS micospheres are obtained at a relatively low temperature of 350 °C (Supporting Information, Figure S6 a–c). With an increase in temperature to 600 °C, the MnS nanocrystals grow into larger-shaped crystals (Supporting Information, Figure S6 d–f). Further increasing the temperature to 800 °C leads to the formation of poorly-defined solid MnS microbricks (Figure S6 g–i). During this process, the shape of the crystals is closely related to their intrinsic crystal structure, reflecting the symmetry of the internal atomic arrangement.[24] However, the initially formed cube-like MnS crystals in each microsphere do not have the same alignment required for the formation of an overall large cubic crystal (Figure 1 b). As a result, irregularly shaped microparticles, instead of microboxes, are eventually formed at high temperature. Similar with microcubes, this evolution is accompanied by a drastic reduction in BET specific surface area from $24.2\ m^2 g^{-1}$ for porous MnS microspheres to only $1.2\ m^2 g^{-1}$ for MnS irregular microparticles (Supporting Information, Figure S4).

As a p-type magnetic semiconductor with a wide bandgap (3.7 eV), MnS has been the subject of extensive studies owing to its many important technological applications.[24–28] When served as one active electrode material in LIBs, the reaction mechanism can be described as follows: $MnS + 2Li^+ \leftrightarrow Mn + Li_2S$. Compared with the currently used graphite (theoretical capacity is 372 mA h g^{-1}), MnS has a much higher theoretical capacity of 616 mA h g^{-1}. Figure 4a shows the representative

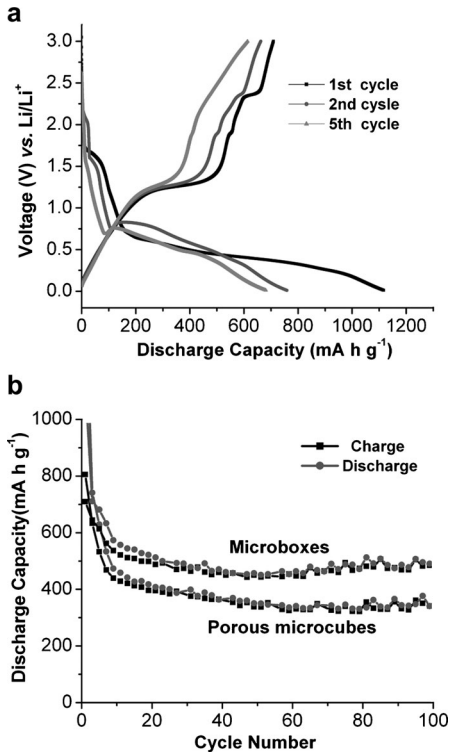

Figure 4. a) Discharge–charge voltage profiles and b) cycling performance of single-crystal MnS microboxes obtained at 800 °C and porous MnS microcubes obtained at 350 °C in the voltage window of 0.01–3.0 V vs. Li/Li$^+$ at a current density of 200 mA g^{-1}.

discharge–charge voltage curves of the MnS microboxes at a current density of 200 mA g^{-1} in the voltage range of 0.01–3.0 V vs. Li/Li$^+$. Discharge capacities of 1117 and 759 mA h g^{-1} are obtained for the first and second cycles, respectively. From the second cycle onwards, the MnS microboxes exhibit excellent cyclic capacity retention, with a stable capacity of about 500 mA h g^{-1}. At the end of 100 charge–discharge cycles, a reversible capacity as high as 495 mA h g^{-1} can still be retained (Figure 4b). As a comparison, the porous MnS microcubes show a much lower discharge capacity, and the capacity drops to 340 mA h g^{-1} at the end of the test (Figure 4b). It is thus apparent that the MnS microboxes manifest much enhanced lithium storage properties compared to porous MnS microcubes and MnS microspheres (see Supporting Information, Figure S7), in terms of both storage capacity and cycling stability. The improved electrochemical performance might be attributed to the higher crystallinity and structural integrity of the MnS microboxes that are obtained at a much higher temperature. Our preliminary results also indicate that the Co-doped and Ni-doped MnS microboxes show significantly improved cycling performance and capacity (Supporting Information, Figure S8).

In summary, we have demonstrated a crystal-structure- and shape-mediated formation mechanism to synthesize MnS microboxes with a single-crystalline shell structure. The MnS microcubes are formed by H_2S gas sulfidation of $MnCO_3$ microcubes at 350–800 °C. With the increase in sulfidation temperature, porous MnS microcubes are first formed at around 350 °C, followed by MnS microcubes with many internal small voids, and finally MnS microboxes with a well-defined single large cavity. Compared with the widely used solution methods, in which the concentration of the precursors is usually very low, the reaction of pre-grown solid precursors with a gas provides a more scalable synthesis of highly uniform hollow structures. When evaluated as potential anode materials for lithium ion batteries, the as-prepared MnS microboxes exhibit high lithium storage capacity and excellent cycling performance.

Experimental Section

A typical synthesis of single-crystalline MnS hollow microcubes was conducted as follows: $MnSO_4{\cdot}H_2O$ (10 mmol), ethanol (70 mL), and $(NH_4)_2SO_4$ (100 mmol) were dissolved in distilled water (700 mL) to form solution A. NH_4HCO_3 (100 mmol) was dissolved in distilled water (700 mL) to form solution B. Solution B was added to solution A under vigorous stirring. The mixed solution was then heated and maintained at 50 °C for 9 h. The white $MnCO_3$ precipitate was collected by filtration, washed thoroughly with distilled water, and dried at 60 °C. To prepare $MnCO_3$ microspheres, no $(NH_4)_2SO_4$ was added and the mixture was kept under stirring for 1 hour at room temperature. To convert the carbonate into MnS, the as-synthesized $MnCO_3$ microcubes were heated to 800 °C with a temperate ramp of 2 °C min^{-1} and kept at the same temperature for 6 h in a flow of 10 % H_2S + 90 % N_2.

X-ray diffraction (XRD) patterns were collected on a Bruker D8 Advanced X-Ray Diffractometer with Ni filtered Cu K_α radiation ($\lambda = 1.5406$ Å) at a voltage of 40 kV and a current of 40 mA. Field-emission scanning electron microscopy (FESEM) images were acquired on a JEOL JSM 6700F microscope operated at 5 kV. Transmission electron microscopy (TEM) images were taken on JEOL 2010 and JEOL 2100 microscopes. Thermogravimetric analysis (TGA) was carried out under nitrogen flow with a temperature ramp of 10 °C min^{-1}. Nitrogen sorption measurements were performed on Autosorb 6B at liquid-nitrogen temperature.

Electrochemical tests were carried out in two-electrode Swagelok cells. The working electrodes consist of 70 % of active material, 20 % of conductive carbon black (Super-P-Li), and 10 % of polymer binder (polyvinylidene fluoride, PVDF). The electrolyte is 1M $LiPF_6$ in a mixture of ethylene carbonate and diethyl carbonate (1:1 by weight). Lithium foil was used as both the counter electrode and reference electrode. Cell assembly was carried out in an argon-filled glovebox with moisture and oxygen concentrations below 1.0 ppm. The charge–discharge tests were performed on a NEWARE battery tester.

Received: April 15, 2012
Published online: June 8, 2012

Keywords: hollow structures · lithium ion batteries · manganese sulfide · microboxes · single crystals

[1] X. W. Lou, L. A. Archer, Z. C. Yang, *Adv. Mater.* **2008**, *20*, 3987.
[2] F. Caruso, R. A. Caruso, H. Mohwald, *Science* **1998**, *282*, 1111.
[3] X. Y. Lai, J. Li, B. A. Korgel, Z. H. Dong, Z. M. Li, F. B. Su, J. A. Du, D. Wang, *Angew. Chem.* **2011**, *123*, 2790; *Angew. Chem. Int. Ed.* **2011**, *50*, 2738.
[4] J. Liu, S. Z. Qiao, S. B. Hartono, G. Q. Lu, *Angew. Chem.* **2010**, *122*, 5101; *Angew. Chem. Int. Ed.* **2010**, *49*, 4981.
[5] H. X. Li, Z. F. Bian, J. Zhu, D. Q. Zhang, G. S. Li, Y. N. Huo, H. Li, Y. F. Lu, *J. Am. Chem. Soc.* **2007**, *129*, 8406.
[6] T. Kim, E. Momin, J. Choi, K. Yuan, H. Zaidi, J. Kim, M. Park, N. Lee, M. T. McMahon, A. Quinones-Hinojosa, J. W. M. Bulte, T. Hyeon, A. A. Gilad, *J. Am. Chem. Soc.* **2011**, *133*, 2955.
[7] S. H. Jiao, L. F. Xu, K. Jiang, D. S. Xu, *Adv. Mater.* **2006**, *18*, 1174.
[8] Y. G. Sun, Y. N. Xia, *Science* **2002**, *298*, 2176.
[9] X. F. Yang, J. X. Fu, C. J. Jin, J. A. Chen, C. L. Liang, M. M. Wu, W. Z. Zhou, *J. Am. Chem. Soc.* **2010**, *132*, 14279.
[10] X. F. Yang, I. D. Williams, J. Chen, J. Wang, H. F. Xu, H. M. Konishi, Y. X. Pan, C. L. Liang, M. M. Wu, *J. Mater. Chem.* **2008**, *18*, 3543.
[11] S. E. Skrabalak, L. Au, X. D. Li, Y. N. Xia, *Nat. Protoc.* **2007**, *2*, 2182.
[12] Y. G. Sun, B. Mayers, Y. N. Xia, *Adv. Mater.* **2003**, *15*, 641.
[13] Z. Y. Wang, D. Y. Luan, F. Y. C. Boey, X. W. Lou, *J. Am. Chem. Soc.* **2011**, *133*, 4738.
[14] Y. M. Sui, W. Y. Fu, Y. Zeng, H. B. Yang, Y. Y. Zhang, H. Chen, Y. X. Li, M. H. Li, G. T. Zou, *Angew. Chem.* **2010**, *122*, 4378; *Angew. Chem. Int. Ed.* **2010**, *49*, 4282.
[15] K. An, S. G. Kwon, M. Park, H. Bin Na, S. I. Baik, J. H. Yu, D. Kim, J. S. Son, Y. W. Kim, I. C. Song, W. K. Moon, H. M. Park, T. Hyeon, *Nano Lett.* **2008**, *8*, 4252.
[16] H. L. Cao, X. F. Qian, C. Wang, X. D. Ma, J. Yin, Z. K. Zhu, *J. Am. Chem. Soc.* **2005**, *127*, 16024.
[17] Y. D. Yin, R. M. Rioux, C. K. Erdonmez, S. Hughes, G. A. Somorjai, A. P. Alivisatos, *Science* **2004**, *304*, 711.
[18] L. Z. Wang, F. Q. Tang, K. Ozawa, Z. G. Chen, A. Mukherj, Y. C. Zhu, J. Zou, H. M. Cheng, G. Q. Lu, *Angew. Chem.* **2009**, *121*, 7182; *Angew. Chem. Int. Ed.* **2009**, *48*, 7048.
[19] T. He, D. R. Chen, X. L. Jiao, Y. L. Wang, *Adv. Mater.* **2006**, *18*, 1078.
[20] H. L. Xu, W. Z. Wang, *Angew. Chem.* **2007**, *119*, 1511; *Angew. Chem. Int. Ed.* **2007**, *46*, 1489.
[21] J. B. Fei, Y. Cui, X. H. Yan, W. Qi, Y. Yang, K. W. Wang, Q. He, J. B. Li, *Adv. Mater.* **2008**, *20*, 452.
[22] H. G. Yang, H. C. Zeng, *J. Phys. Chem. B* **2004**, *108*, 3492.
[23] X. W. Lou, Y. Wang, C. L. Yuan, J. Y. Lee, L. A. Archer, *Adv. Mater.* **2006**, *18*, 2325.
[24] A. Puglisi, S. Mondini, S. Cenedese, A. M. Ferretti, N. Santo, A. Ponti, *Chem. Mater.* **2010**, *22*, 2804.
[25] S. Biswas, S. Kar, S. Chaudhuri, *J. Cryst. Growth* **2005**, *284*, 129.
[26] G. Pandey, H. K. Sharma, S. K. Srivastava, R. K. Kotnala, *Mater. Res. Bull.* **2011**, *46*, 1804.
[27] Q. W. Tian, M. H. Tang, F. R. Jiang, Y. W. Liu, J. H. Wu, R. J. Zou, Y. G. Sun, Z. G. Chen, R. W. Li, J. Q. Hu, *Chem. Commun.* **2011**, *47*, 8100.
[28] N. Zhang, R. Yi, Z. Wang, R. R. Shi, H. D. Wang, G. Z. Qiu, X. H. Liu, *Mater. Chem. Phys.* **2008**, *111*, 13.

